Silicon and zinc biogeochemical cycles coupled through the Southern Ocean

Derek Vance[1*], Susan H. Little[2], Gregory F. de Souza[1], Samar P. Khatiwala[3], Maeve C. Lohan[4], Rob Middag[5]

[1]Institute of Geochemistry and Petrology, Department of Earth Sciences, ETH Zürich, Clausiusstrasse 25, 8092 Zürich.

[2]Department of Earth Science and Engineering, Imperial College London, South Kensington Campus, Exhibition Road, London, SW7 2AZ, UK.

[3]Department of Earth Sciences, South Parks Road, Oxford, OX1 3AN, UK.

[4]School of Ocean and Earth Sciences, National Oceanography Centre, University of Southampton, Southampton, UK.

[5]Royal Netherlands Institute for Sea Research (Royal NIOZ), P.O. Box 59, 1790 AB Den Burg, Texel, The Netherlands.

Zinc is vital for the physiology of oceanic phytoplankton. The striking similarity of the depth profiles of zinc to those of silicate suggests that the uptake of both elements into the opaline frustules of diatoms, and their regeneration from these frustules, should be coupled. However, the zinc content of diatom opal is negligible, and zinc is taken up into and regenerated from the organic parts of diatom cells. Thus, since opaline frustules dissolve deep in the water column whilst organic material is regenerated in the shallow subsurface ocean, there is little reason to expect the observed close similarity between zinc and silicate, and the dissimilarity between zinc and phosphate. Here we combine observations with simulations using a three-dimensional model of ocean circulation and biogeochemistry to show that the coupled distribution of zinc and silicate, as well as the decoupling of zinc and phosphate, can arise in the absence of mechanistic links between the uptake of zinc and silicate, and despite contrasting regeneration length-scales. Our simulations indicate that the oceanic zinc distribution is, in fact, a natural result of the interaction between ocean biogeochemistry and the physical circulation through the Southern Ocean hub. Our analysis demonstrates the importance of uptake stoichiometry in controlling ocean biogeochemistry, and the utility of global-scale elemental co-variation in the ocean in understanding these controls.

The spatial and vertical distributions of macro- (e.g. phosphate, nitrate, silicate) and metal micro-nutrients (e.g. iron, zinc) control sequestration of carbon by the ocean's biosphere. Zinc plays vital physiological roles in oceanic phytoplankton (e.g., ref 1) and Zn contents of phytoplankton cells are of the same order as the essential trace element, iron[2-4]. As a result, and like the major nutrients (P, N, Si), Zn shows extreme depletions in the surface ocean and enrichments at depth (Fig. 1, see Fig. 2 for locations and sources of all data used in the paper), a distribution that is often conceptualised in terms of one-dimensional vertical cycling involving uptake in the photic zone and regeneration beneath. Though the extent to which surface Zn concentrations limit primary productivity is still unclear (e.g., ref 12), the processes that control the removal of Zn from the photic zone, its

regeneration in the deep ocean, and its return to the surface via the ocean circulation, are a key part of the dynamics of oceanic nutrient chemistry.

A remarkable feature of global ocean nutrient profiles (Fig. 1) is the tight co-variation of Zn and Si in all three major ocean basins. Both elements increase to maxima for each profile in the abyssal ocean, in marked contrast to the intermediate-depth maximum for PO_4. Though this coupling of Zn to Si has been repeatedly noted[5-7], its origin has been a puzzle. Rationales for the deep maximum in Si relative to organic-associated nutrients, nitrate and phosphate, have emphasised two key processes: (1) vertical cycling with a greater regeneration length-scale of diatom opal relative to organic matter (e.g., 13, 14); (2) rapid depletion of Si relative to organic-associated nutrients in the surface Southern Ocean, creating distinct water mass signatures that are exported to the rest of the global ocean[15,16]. For Zn it has been tentatively suggested that uptake of Zn and Si may be linked, and that increased Si uptake by diatoms due to Fe limitation may explain co-variation of Zn and Si observed in high-latitude nutriclines[17]. The first of these two views would suggest that the oceanic cycle of Zn is dominated by uptake into and regeneration from diatom opal. However, culturing studies[18] have demonstrated that the Zn content of diatom opal is negligible (1-3% of the total cellular inventory), and that the Zn/Si ratio of diatom opal is nearly two orders of magnitude lower than observed in the deep ocean[5,18]. This is confirmed by synchrotron micro-XRF data[2,3] from both cultured and natural diatom cells, which clearly show that Zn is co-located with phosphorus in the organic matter of diatom cells and not in their opaline frustules, and that Zn is regenerated from this organic material in the upper ocean with phosphate, and not with Si from opal[19,20].

Diatom uptake in the Southern Ocean couples Zn and Si

We suggest that the solution to this paradox lies in the biogeochemistry and physical oceanography of the Southern Ocean. Water upwelled at the Antarctic divergence, and moved northward at the

surface by Ekman transport to the Sub-Antarctic zone, is stripped of Si and Zn much faster than PO_4 (Fig. 3a, b). Thus, both Zn and Si concentrations drop by a factor of about 40 over the surface transect shown in Fig. 3a, whereas PO_4 drops by only a factor of 3. This remarkable difference in relative drawdown rates is consistent with the ecological dominance of diatoms in this region (e.g. refs 22, 23), and their peculiarly high Zn/P uptake ratio, up to an order of magnitude greater than the average for oceanic phytoplankton[3]. The Zn- and Si-depleted Sub-Antarctic surface layer is the ultimate source of Sub-Antarctic Mode Water (SAMW), and it is the northward transport of this water mass that, we suggest, sets the low dissolved Si and Zn concentrations, and low Si/PO_4 and Zn/PO_4 ratios, of most of the global upper ocean (Fig. 1). The data in Fig. 3a also imply a rather constant ratio for the removal of Zn and Si from the dissolved pool of the surface Southern Ocean, despite the fact that Si is taken up into opal and Zn into organic material.

What is the ultimate fate of the large amounts of Zn and Si relative to PO_4 removed from the surface Southern Ocean? The Sub-Antarctic winter mixed layer from which SAMW forms is of the order of 200-400m thick (e.g., ref 24), beneath which the Southern Ocean water column is vigorously mixed and rather homogeneous (e.g., ref 25), including for Si, Zn and PO_4[11]. Thus, if diatom cells are exported beneath about 200-400m, their high Zn/P and Si/P characteristics will be imparted to the deep Southern Ocean regardless of the exact cellular location (opal or organic matter) of Zn, Si and P, making the different regeneration length-scales of these particulate phases much less relevant here than elsewhere in the ocean. This export, which may be aided by the rapid blooming and equally rapid population collapse that is characteristic of diatom ecology (e.g., refs 22, 23), results in a Zn and Si deficit relative to PO_4 in the mixed layer, which is the source of upper ocean water masses such as AAIW and SAMW.

In summary, the hypothesis we put forward here consists of three components: (1) extreme drawdown of Zn and Si relative to PO_4 in the surface Southern Ocean (Fig. 2a) consistent with the known stoichiometry of Southern Ocean diatoms[3], thus setting the biogeochemical signature of the surface Southern Ocean and the upper ocean water masses derived from it; (2) export of diatom cells below the winter mixed layer depth, transferring both Zn and Si at high Zn/P and Si/P to the deep Southern Ocean, despite being located in two different components of the diatom cell with different regeneration length-scales, thus setting the biogeochemical signatures of deep and abyssal Southern Ocean-derived water masses (Fig. 1); and (3) lateral export of these water mass signatures to the low latitude oceans, as previously proposed to control Si-NO_3 nutrient systematics[15,16]. The imprint of these processes can be seen in Fig. 3c. Zinc-PO_4 data for the Atlantic sector of the Antarctic zone of the Southern Ocean (including the surface transect in Fig. 3a and the entire water column at 67°S, black triangles[11]) indicate co-variation along a line with a slope of about 8 mmol mol^{-1}, consistent with a control by diatom uptake and regeneration. Data for stations proximal to the Southern Ocean, at 40°S in the South Atlantic (entire water column, blue squares[7]) clearly show two different behaviours, with the deep ocean lying close to the Antarctic zone data, and the upper ocean data reflecting the much lower slope expected for water masses sourced in the mixed layer of the Southern Ocean, from which Zn has been stripped. The red dashed lines indicate, schematically, how water mass mixing in locations more distal from the Southern Ocean sources would confound these clear distinctions.

The Southern Ocean uptake hypothesis tested in an ocean model

To provide a quantitative test of these ideas, and taking advantage of the computational efficiency of the transport matrix method[26], we performed a series of 11 sensitivity simulations (see Methods and Supplementary Information) using an ocean general circulation model coupled offline to a biogeochemical model of P, Si and Zn cycling. In the biogeochemical model, PO_4 and Si cycling

are treated completely independently, whilst Zn cycling is explicitly tied to that of P. Zinc in the oceanic dissolved pool is present as both inorganic Zn (Zn') and complexed with an organic ligand (ZnL). Culturing studies[27] have shown that Zn uptake by phytoplankton, and their Zn/P ratios, can be parameterised using the quantitative dependence of Zn uptake on free Zn concentrations, the approach we adopt here. It is currently unclear exactly *why* Southern Ocean diatoms exhibit high Zn/P uptake ratios, but the high values seen in data[3] emerge from the model simply from the fact that upwelled water in the Southern Ocean contains high concentrations of Zn so that not all of it is complexed by organic ligands, a finding that is also supported by data[28].

Although the lengthscale of Zn regeneration is identical to P in these simulations, and though its cycling is entirely decoupled from that of Si, our model reproduces the observed near-linear correlation between Zn and Si at the global scale (Fig. 4c). It also reproduces the slow increase with depth in Zn concentrations through the upper ocean at low latitudes (Fig. 1), despite the fact that Zn is regenerated in the shallow subsurface in the model. The mechanism behind this model behaviour is indicated by our model's sensitivity to the Zn/P uptake ratio in the Southern Ocean (see Supplementary Information for sensitivity tests): as the average Zn/P ratio of uptake in the Southern Ocean increases, the Zn distribution changes from being closely correlated with that of PO_4 (at Zn/P uptake ratios of ~1 mmol mol^{-1}) to being very similar to the large-scale Si distribution (at values above ~4.5 mmol mol^{-1}).

The key feature of the global Zn-PO_4 covariation (Fig. 4d) is the curvature in the model array. This arises because of the partitioning of the global oceans into the two broad regimes seen in Fig. 3c: an upper ocean that is severely depleted in Zn (and Si) relative to PO_4 as a result of the stripping of Zn (and Si) from the surface Southern Ocean, and the export of this water to the upper ocean globally; and a deep and abyssal ocean that is dominated by water masses originating in the deep Southern

147 Ocean, containing the regenerated counterpart of this surface uptake process. The model is less
148 good at representing the physical mixing of these end-members outside the Southern Ocean (see
149 schematic trajectories in Fig. 3c), so that it underestimates the scatter in the data in Fig. 4b,d.
150
151 We emphasise that our aim here is to provide an explanation for a first-order feature of global ocean
152 Zn-Si-P distributions and, as such, we have deliberately kept the model simple, attempting to
153 restrict the processes it represents to those that are well-established. Thus, Zn uptake is tied to that
154 of P as dictated by the results of culturing experiments, and there are no mechanistic links between
155 the uptake of Zn and Si. We have paramaterised Zn speciation in the context of a single ligand
156 model (see Supplementary Information). The model does not consider the potential impacts of
157 variations in metal uptake stoichiometry across different taxonomic groups. It does not consider the
158 potential effects that Fe limitation may have on diatom physiology. Despite this simplicity, the
159 model is very successful in reproducing global dissolved nutrient distributions. Invoking further
160 complexity, such as a significant role for previously-proposed vertical processes such as scavenging
161 of Zn by particulate material or a second organic Zn pool associated with opal[11,29,30] is not required
162 to reproduce first-order global Zn-Si-PO_4 relationships. We have also avoided tuning the model to
163 improve the fit to the data. For example, the slope of the model Zn-Si correlation on Fig. 4c is about
164 12% below that defined by the data, at 0.056 mmol mol^{-1} versus 0.064 mmol mol^{-1}. The simulated
165 slope is entirely dependent on assumed model values for the average oceanic Zn and Si
166 concentrations, drawn from the literature (see Supplementary Information). The former, in
167 particular, given the comparative lack of data coverage, is certainly only an estimate at this stage.
168
169 Our analysis of Zn-Si-PO_4 systematics in the global ocean has important implications for both Zn
170 itself and for oceanic trace elements more broadly. The implication of our proposal is that Southern
171 Ocean diatoms dominate oceanic Zn cycling, transferring a large fraction of the oceanic pool to the

abyssal ocean and trapping it there, in a direct analogy with Si trapping[15,16]. The finding that Zn distributions in the global ocean are so profoundly influenced by the stoichiometry of uptake in the Southern Ocean has relevance for studies of other trace metals, their oceanic distributions, and relationships between different nutrients. For example, the "kink" in Zn-PO_4 is reminiscent of the well established "kink" in the relationship between the trace metal cadmium (Cd) and PO_4, whose precise origin is much debated[31-33]. Phytoplankton uptake stoichiometry, speciation of metals in the photic zone, and their systematics in regions of the ocean that are hubs for the physical circulation, are likely as important for other metals as they are for Zn in determining global ocean distributions. The implication is that oceanic metal micronutrient distributions are set by a combination of Southern Ocean ecology and physical circulation, as for major nutrients[15,16]. Therefore, changes in the Southern Ocean forced by past and future climate change will have global impact.

References

1. Morel, F.M.M., Milligan, A.J. & Saito, M.A. Marine bioinorganic chemistry: the role of trace metals in the oceanic cycles of major nutrients. *Treatise in Geochemistry* **8**, 123-150 (2014).

2. Twining, B.S. *et al.* Quantifying trace elements in individual aquatic protest cells with a synchrotron X-ray fluorescence microprobe. *Anal. Chem.* **75**, 3806-3816 (2003).

3. Twining, B.S. & Baines, S.B. The trace metal composition of marine phytoplankton. *Ann. Rev. Mar. Sci.* **5**, 191-215 (2013).

4. Boyd, P.W. & Ellwood, M.C. The biogeochemical cycle of iron in the ocean. *Nature Geoscience* **3**, 675-682 (2010).

5. Bruland, K.W. Oceanographic distributions of cadmium, zinc, nickel, and copper in the North Pacific. *Earth Planet. Sci. Lett.* **47**, 176-198 (1980).

6. Martin, J.H., Gordon, R.M., Fitzwater, S. & Broenkow, W.W. VERTEX: phytoplankton/iron studies in the Gulf of Alaska. *Deep-Sea Res.* **36**, 649-680 (1989).

7. Wyatt, N.J. *et al.* Biogeochemical cycling of dissolved zinc along the GEOTRACES South Atlantic transect GA10 at 40°C. *Glob. Biogeochem. Cycles* **28**, 44-56 (2014).

8. You, Y. Intermediate water circulation and ventilation of the Indian Ocean derived from water-mass contributions. *J. Mar.Res.* **56**, 1029-1067 (1998).

9. Vu, H.T.D. & Sohrin, Y. Diverse stoichiometry of dissolved trace metals in the Indian Ocean. *Sci. Rep.* **3**, paper 1745. (2013).

10. Geotraces Intermediate Data Product. http://www.bodc.ac.uk/geotraces/data/idp2014.

11. Zhao, Y., Vance, D., Abouchami, W. & de Baar, H.J.W. Biogeochemical cycling of zinc and its isotopes in the Southern Ocean. *Geochim. Cosmochim. Acta* **125**, 653-672 (2014).

12. Moore, C.M. *et al.* Processes and patterns of oceanic nutrient limitation. *Nature Geosci.* 6, 701-710. (2013).

207 13. Berelson, W.M. The flux of particulate organic carbon into the ocean interior: a comparison of
208 four US JGOFS regional studies. *Oceanogr.* **14**, 59-67 (2001).
209 14. Ragueneau, O., Dittert, N., Pondaven, P., Treguer, P. & Corrin, L. Si/C decoupling in the world
210 ocean: is the Southern Ocean different? *Deep-Sea Research II* **49**, 3127-3154 (2002).
211 15. Sarmiento, J.L., Gruber, N., Brzezhinski, M.A. & Dunne, J.P. High latitude controls of
212 thermocline nutrients and low latitude biological productivity. *Nature* **427**, 56-60 (2004).
213 16. Sarmiento, J.L. *et al.* Deep ocean biogeochemistry of silicic acid and nitrate. *Global*
214 *Biogeochem. Cycles* **21**, B1S90, 10.1029/2006GB002720 (2007).
215 17. Sunda, W.G. & Huntsman, S.A. Effect of Zn, Mn, and Fe on Cd accumulation in
216 phytoplankton: implications for oceanic Cd cycling. *Limnol. Oceanogr.* **45**, 1501-1516 (2000).
217 *Limnol. Oceanogr.* **59**, 689-704 (2014).
218 18. Ellwood, M.C. & Hunter, K.A. The incorporation of zinc and iron in the frustule of the marine
219 diatom *Thalassiosira pseudonana*. *Limnol. Oceanogr.* **45**, 1517-1524 (2000).
220 19. Lee, B.-G. & Fisher, N.S. Release rates of trace elements and protein from decomposing
221 planktonic debris. I. Phytoplankton debris. *J. Mar. Res.* **51**, 391-421 (1993).
222 20. Twining, B.S. *et al.* Differential remineralization of major and trace elements in sinking
223 diatoms.
224 21. Schlitzer, R. Electronic atlas of WOCE hydrographic and tracer data now available. *EOS Trans.*
225 *AGU* **81**, 45 (2000).
226 22. Armbrust, E.V. The life of diatoms in the world's oceans. *Nature* **459**, 185-192 (2009).
227 23. Assmy, P. et al. Thick-shelled grazer-protected diatoms decouple ocean carbon and silicon cycle
228 in the iron-limited Antarctic Circumpolar Current. *Proc. Natl. Acad. Sci.* **51**, 20633-20638 (2013).
229 24. Sallée, J. B., Wienders, N., Speer, K. & Morrow, R. Formation of subantarctic mode water in
230 the southeastern Indian Ocean. *Ocean Dyn.* **56**, 525–54. (2006).

231 25. Marshall, J. & Speer, K. Closure of the meridional overturning circulation in the Southern
232 Ocean. *Nature Geosci.* **5**, 171-180 (2012).
233 26. Khatiwala, S., Visbeck, M. & Cane, M.A. Accelerated simulation of passive tracers in ocean
234 circulation models. *Ocean Modelling* **9**, 51-69 (2005).
235 27. Sunda, W.G. & Huntsman, S.A. Feedback interactions between zinc and phytoplankton in
236 seawater. *Limnol. and Oceanogr.* **37**, 25-40 (1992).
237 28. Baars, O. & Croot, P.L. The speciation of dissolved zinc in the Atlantic sector of the Southern
238 Ocean. *Deep Sea Res. II* **58**, 2720-2732 (2011).
239 29. Lohan, M.C., Statham, P.J. & Crawford, D.W. (2002) Total dissolved zinc in the upper water
240 column of the subarctic North East Pacific. *Deep-Sea Res. II* **49**, 5793-5808 (2002).
241 30. John, S.G. & Conway, T.M. A role for scavenging in the marine biogeochemical cycling of zinc
242 and zinc isotopes. *Earth Planet. Sci. Lett.* **394**, 159-167 (2014).
243 31. Elderfield, H. & Rickaby, R.E.M. Oceanic Cd/O ratio and nutrient utilization in the Southern
244 Ocean. *Nature* **405**, 305-210 (2000).
245 32. Cullen, J.T. On the nonlinear relationship between dissolved cadmium and phosphate in the
246 modern global ocean: could chronic iron limitation of phytoplankton growth cause the kink?
247 *Limnol. Oceanogr.* **51**, 1369-1380 (2006).
248 33. Quay, P., Cullen, J.T., Landing, W.M. & Morton, P. Processes controlling the distributions of
249 Cd and PO_4 in the ocean. *Glob. Biogeochem. Cyc.* **29**, 830-841. (2015)
250
251 Correspondence and requests for materials to: derek.vance@erdw.ethz.ch.
252
253 **Acknowledgements**

This research was supported by ETH Zürich and Swiss National Science Foundation (SNF) Grant 200021-153087/1 to DV. SHL is supported by a Leverhulme Early Career Fellowship and GFdS by a Marie Sklodowska-Curie Fellowship.

Author contributions

DV and SHL conceived the study. DV wrote the first draft of the paper. GdS constructed the biogeochemical model in collaboration of SPK, conceived and carried out the sensitivity simulations, and analysed the model output. MCL and RM were responsible for the Atlantic data in the GEOTRACES Intermediate Data Product and used in the figures. All authors read and commented on the paper.

Competing financial interests

The authors declare no competing financial interests.

Figure captions

Figure 1: Example depth profiles of Zn, Si and PO_4 in the three main ocean basins

The striking similarity in the depth distributions of Zn and Si stands in marked contrast to the dissimilarity with PO_4. The presence of Sub-Antarctic Mode Water (SAMW, potential density anomaly σ_θ = 26.80[15]) and Antarctic Intermediate Water (AAIW[7,8]) in the South Atlantic and equatorial Indian Oceans is reflected in the low Si and Zn concentrations compared to P. In the North Pacific these depth levels are occupied by other water masses. Locations of stations depicted, as well as data sources, are given in Fig. 2.

Figure 2: Location map

The locations of the stations from which nutrient data are depicted in Figs. 1, 3 and 4. Pacific data from Bruland et al.[5] (Station 17) and VERTEX profiles[6]. Atlantic (GA02 and GA10[7]) and Indian (GI04[9]) data from the GEOTRACES 2014 Intermediate Data Product[10]. Southern Ocean (IPY) data from Zhao et al.[11].

Figure 3: Contrasting variability in nutrient uptake in the Atlantic sector of the Southern Ocean

a,b: The strong depletion of Zn and Si versus moderate depletion of PO_4 as water is moved northward from the upwelling zone (data from dashed black line in Fig. 2[7,11]). Physical features identified using WOCE hydrographic data along the zero meridian[21]: AD, Antarctic Divergence; PF, Polar Front; SAF, Sub-Antarctic Front; AZ, Antarctic Zone, PFZ, Polar Frontal Zone; SAZ, Sub-Antarctic Zone. **c:** Distribution of Zn and PO_4 in the Atlantic sector of the Southern Ocean. Antarctic Zone data[11] track removal of Zn and PO_4 at a very high ratio (Zn/P = 8 mmol mol^{-1}). South Atlantic 40°S data[7] show contrasting Zn/P ratios, extremely low (0.3 mmol mol^{-1}) in the upper ocean, and high in the deep. Dashed red lines show possible trajectories for mixing between end-members on this diagram.

Figure 4: Coupled major and micro-nutrient distributions in the global ocean

a,b: Global Zn-Si-PO_4 systematics in all three ocean basins. Black arrows in **b** as in Fig 3c. Data plotted for all stations on each section shown in Fig. 2 (see caption for data sources), and for the entire water column. **c,d:** The same data as in **a,b** (grey), with the results of a three-dimensional model of ocean circulation and biogeochemistry superimposed (Simulation 11, see Supplementary

301 Information; colours represent the volume-weighted relative frequency of model cells with the
302 given Zn-Si or Zn-PO_4 characteristics).
303

Methods

Physical model: Ocean general circulation model simulations were carried out using the transport matrix method (TMM) of Khatiwala et al.[26] using transport matrices (TMs) derived from a coarse-resolution version of the MITgcm[34] with 2.8° × 2.8° lateral resolution and 15 vertical levels forced with monthly mean climatological fluxes of momentum, heat and freshwater and with weak restoring of surface temperature and salinity to the Levitus climatology[35]. Our sensitivity simulations were carried out using constant annual-mean circulation fields derived from the equilibrium state of the model after 5000 yr integration; thus, seasonal variability is not represented in our simulations. The physical model is coupled to a biogeochemical model that simulates the internal oceanic cycling of phosphorus (as phosphate, PO_4, and dissolved organic phosphorus, DOP), zinc (Zn) and silicate (Si). Biogeochemical model simulations were initialized with constant nutrient tracer fields (ocean-mean concentrations of 2.17 μM, 5.4 nM and 92 μM for PO_4, Zn and Si respectively) and integrated forward for 5000 model years.

Biogeochemical model: The nutrient-cycling model that forms the basis of our simulations is based on the formulation developed for the OCMIP-2 project[36] and uses PO_4 as its nutrient currency. Phosphate uptake in the surface ocean is driven by restoring surface PO_4 concentrations[37,38] towards the objectively-analysed annual-mean PO_4 field of World Ocean Atlas 2013[39] with a restoring timescale of 36.5 days. A fraction of PO_4 taken up is immediately shunted towards DOP, whilst the remaining fraction is exported as an implicit particulate flux to depth, which remineralises following a power-law dependency on depth[40,41]. Any particulate flux reaching the bottom of the water column remineralises within the bottom ocean cell. Dissolved organic phosphorus is carried passively with the circulation and decays back to PO_4 with a first-order rate constant of $(0.5\ \text{year})^{-1}$.

The Zn-cycling model is explicitly coupled to the P-cycling model above. Zinc uptake in the surface ocean is tied to PO_4 uptake via a dimensionless stoichiometric parameter $r_{Zn:P}$ (see *Zn uptake parameterization* below). This surface-ocean uptake drives an implicit export flux of

particulate Zn, which remineralises identically to the implicit particulate P flux. The organic speciation of dissolved Zn is represented implicitly by assuming a constant ligand concentration of 1.2 nM with a conditional stability constant of 10^{10} M^{-1}, which reduces the calculation of the concentration of free Zn (i.e. organically and inorganically uncomplexed Zn^{2+}) to the solution of a quadratic equation (see Supplementary Information). Varying biogeochemical behaviours of the Zn-cycling model are achieved by the formulation of the stoichiometric parameter $r_{Zn:P}$, as detailed below.

Our silicon cycling model is conceptually very similar to our PO_4-cycling model, and to the Si-cycling model of de Souza et al.[42]. Dissolved Si uptake in the surface ocean (≤ 120m water depth) is driven by restoring surface Si concentrations towards the objectively-analysed annual-mean Si field of World Ocean Atlas 2013 with a restoring timescale of 36.5 days. This surface-ocean uptake drives an implicit particulate export flux, which dissolves following an exponential dependency on depth with a length-scale of 1000 m (ref. 41). Any particulate flux reaching the bottom of the water column remineralises within the bottom ocean cell. It is important to note that in our model formulation, Si cycling is entirely biogeochemically independent of PO_4 and Zn cycling.

Zn uptake parameterization

Details of the parameterization of Zn uptake, including the rationale behind choices made in defining this parameterization, can be found in the Supplementary Information. Broadly, our biogeochemical model represents the plasticity in the Zn:P stoichiometry of uptake by phytoplankton (diatoms and coccolithophorids) observed in culture experiments by Sunda and Hunstman[27]. These authors observed that the Zn:P uptake ratio varies non-linearly with the concentration of free Zn (Zn^{2+}) in the culturing medium, a dependency with the following functional form (called the "two-site model"):

$$r_{Zn:P} = \frac{a_{Zn} \cdot Zn^{2+}}{b_{Zn} + Zn^{2+}} + c_{Zn} \cdot Zn^{2+} \qquad \text{(Eqn. 1)}$$

where $r_{Zn:P}$ is the molar Zn:P uptake ratio, and parameters a_{Zn}, b_{Zn} and c_{Zn} are constants analogous to maximum uptake rate, half-saturation constant and non-saturable uptake rate, respectively. The culture data of Sunda and Huntsman[26] were used to delineate the extent of variability of these parameters in our suite of sensitivity simulations, as detailed in the Supplementary Information. Parameters and key statistical metrics for the 11 sensitivity simulations carried out are listed in Table S1, together with a detailed discussion of the results.

Data availability. The data that support the findings of this study are available at http://www.bodc.ac.uk/geotraces/data/idp2014.

Code availability. The TMM code is available on GitHub (https://github.com/samarkhatiwala/tmm), and the biogeochemical code can be provided on request.

References

34. Marshall, J., Adcroft, A., Hill, C., Perelman, L. & Heisey, C. A finite-volume, incompressible Navier-Stokes model for studies of the ocean on parallel computers. *J. Geophys. Res. Oceans* **102**, 5733-5752 (1997).

35. Levitus, S., et al. World Ocean Database 1998, NOAA Atlas NESDIS 18, NOAA, Silver Spring, MD (1998).

36. Najjar, R.G., et al. Impact of circulation on export production, dissolved organic matter, and dissolved oxygen in the ocean: Results from Phase II of the Ocean Carbon-cycle Model Intercomparison Project (OCMIP-2). *Glob. Biogeochem. Cyc.* **21**, GB3007, doi: 10.1029/2006gb002857 (2007).

376 37. Najjar, R.G., Sarmiento, J.L. & Toggweiler, J.R.. Downward transport and fate of organic
377 matter in the ocean: Simulations with a general circulation model. *Glob. Biogeochem. Cyc.* **6**, 45-76
378 (1992).
379 38. Anderson, L.A. & Sarmiento, J.L. Global ocean phosphate and oxygen simulations. *Glob.*
380 *Biogeochem. Cyc.* **9**, 621-636 (1995).
381 39. Garcia, H.E., Locarnini, R.A., Boyer, T.P., Antonov, J.I., Baranova, O.K., Zweng, M.M.,
382 Reagan, J.R. & Johnson, D.R.. World Ocean Atlas 2013, Volume 4: Dissolved Inorganic Nutrients
383 (phosphate, nitrate, silicate), Levitus, S. (Ed.), NOAA Atlas NESDIS 76, Silver Spring, MD (2013).
384 40. Martin, J.H., Knauer, G.A., Karl, D.M. & Broenkow, W.W.. VERTEX: carbon cycling in the
385 northeast Pacific. *Deep Sea Res.* **34**, 267-285 (1987).
386 41. Berelson, W.M. The flux of particulate organic carbon into the ocean interior: a comparison of
387 four US JGOFS regional studies. *Oceanogr.* **14**, 59-67 (2001).
388 42. de Souza, G.F., Slater, R.D., Dunne, J.P. & Sarmiento, J.L. Deconvolving the controls on the
389 deep ocean's silicon stable isotope distribution. *Earth Planet. Sci. Lett.* **398**, 66-76 (2014).

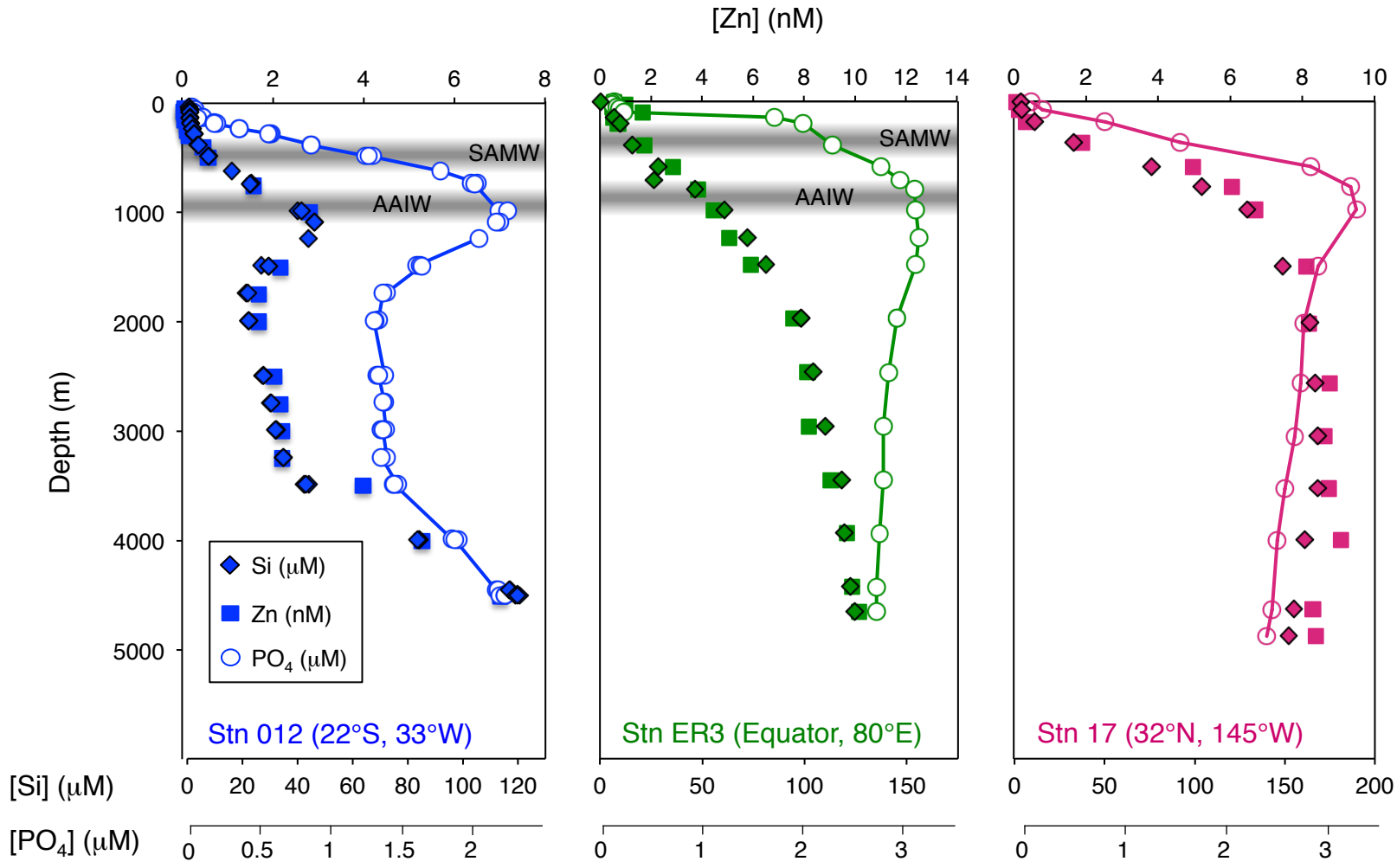
[Zn] (nM)
Depth (m)
SAMW
AAIW
Si (μM)
Zn (nM)
PO4 (μM)
Stn 012 (22°S, 33°W)
Stn ER3 (Equator, 80°E)
Stn 17 (32°N, 145°W)
[Si] (μM)
[PO4] (μM)

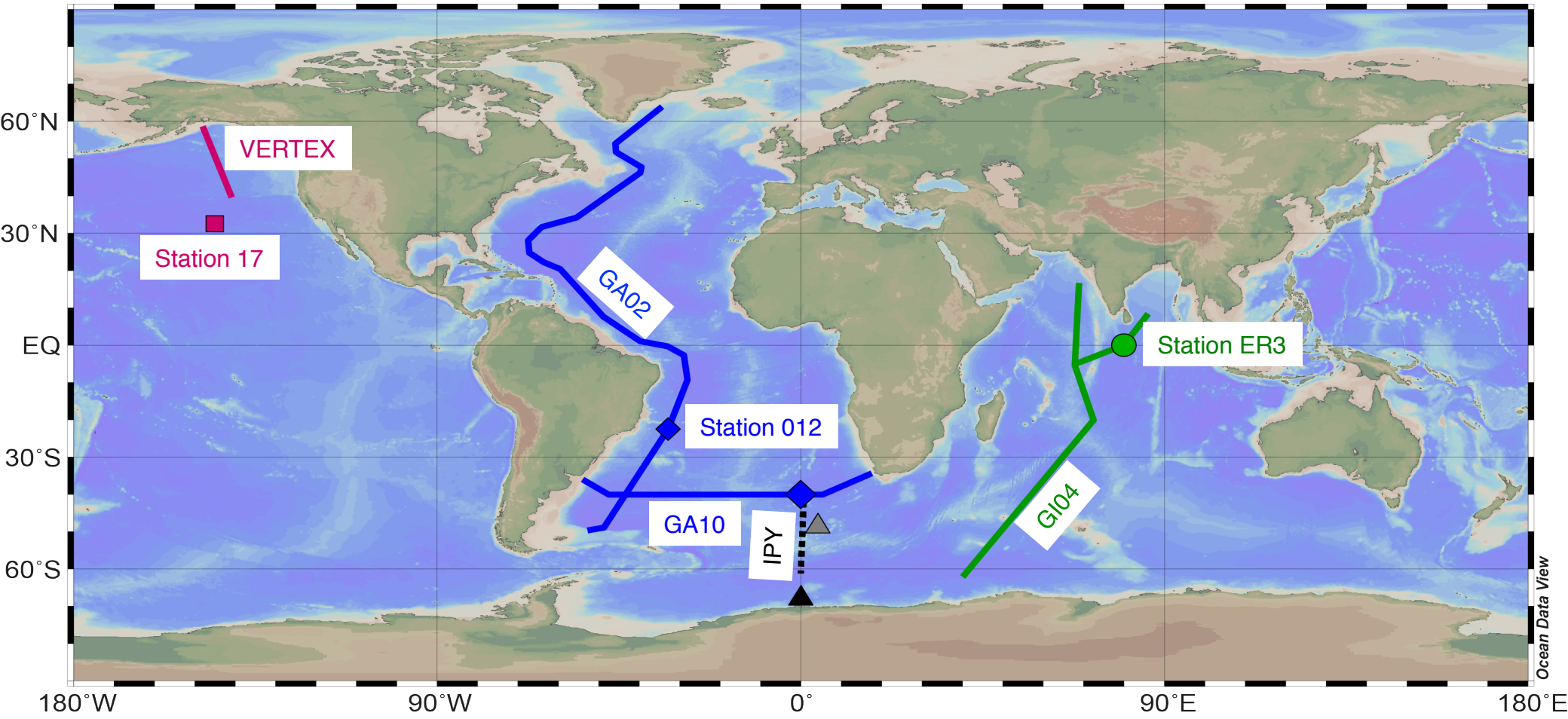
VERTEX
Station 17
GA02
Station 012
GA10
IPY
Station ER3
GI04
60˚N
30˚N
EQ
30˚S
60˚S
180˚W
90˚W
0˚
90˚E
180˚E
Ocean Data View

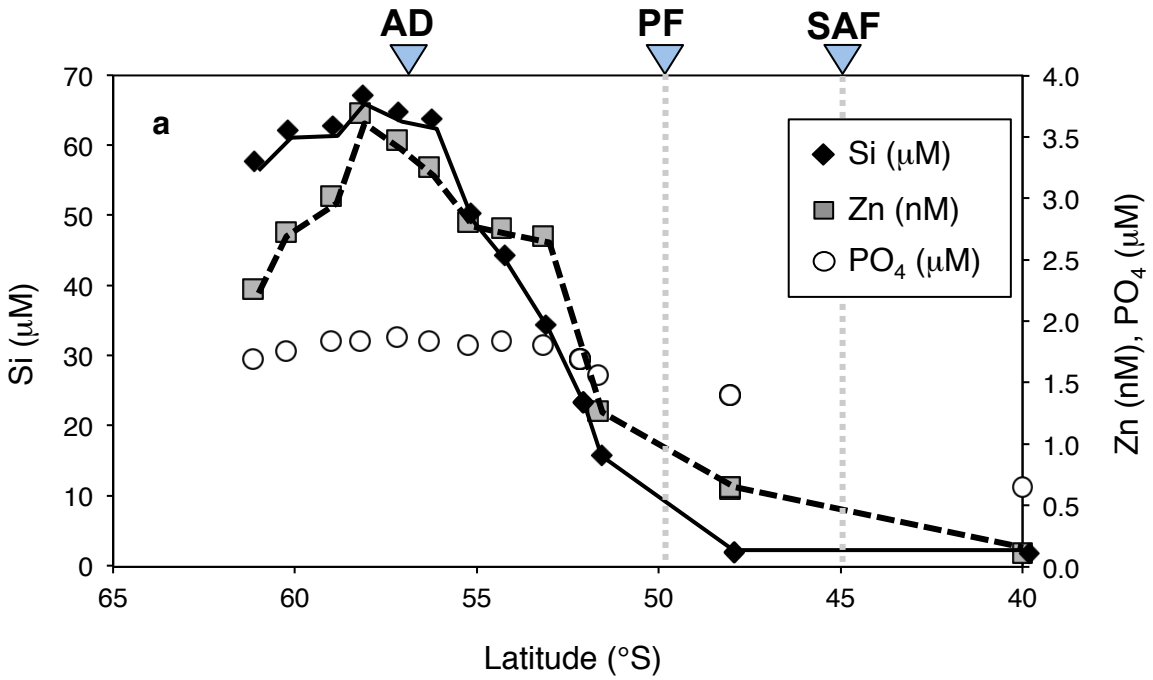
AD
PF
SAF
a
Si (μM)
Zn (nM)
PO4 (μM)
Si (μM)
Zn (nM), PO4 (μM)
Latitude (°S)

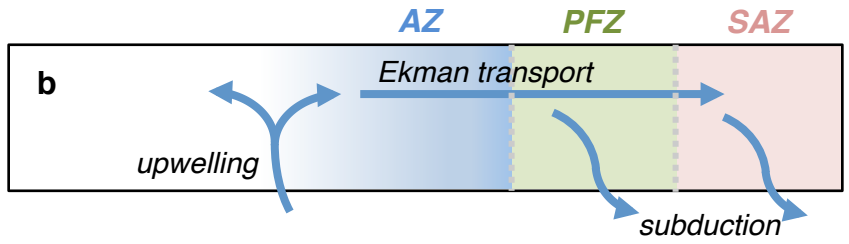
AZ
PFZ
SAZ
b
Ekman transport
upwelling
subduction

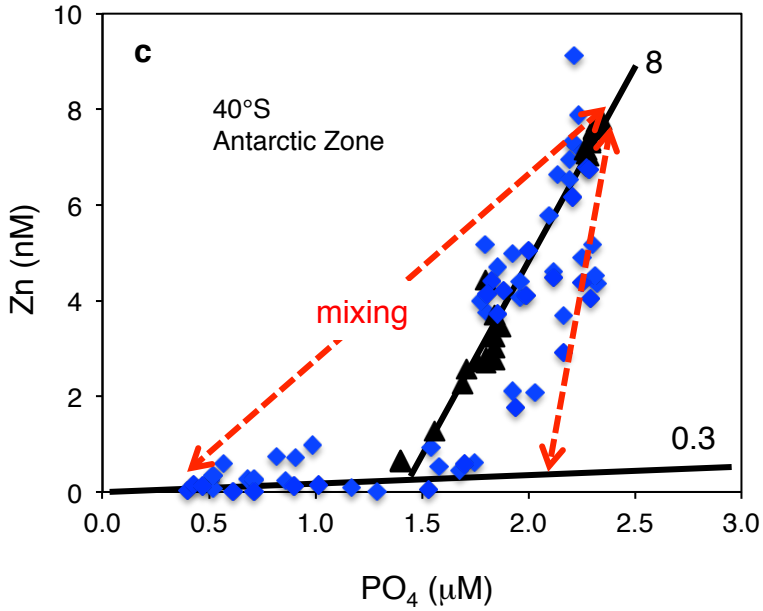
c
40°S
Antarctic Zone
mixing
8
0.3
Zn (nM)
PO4 (μM)

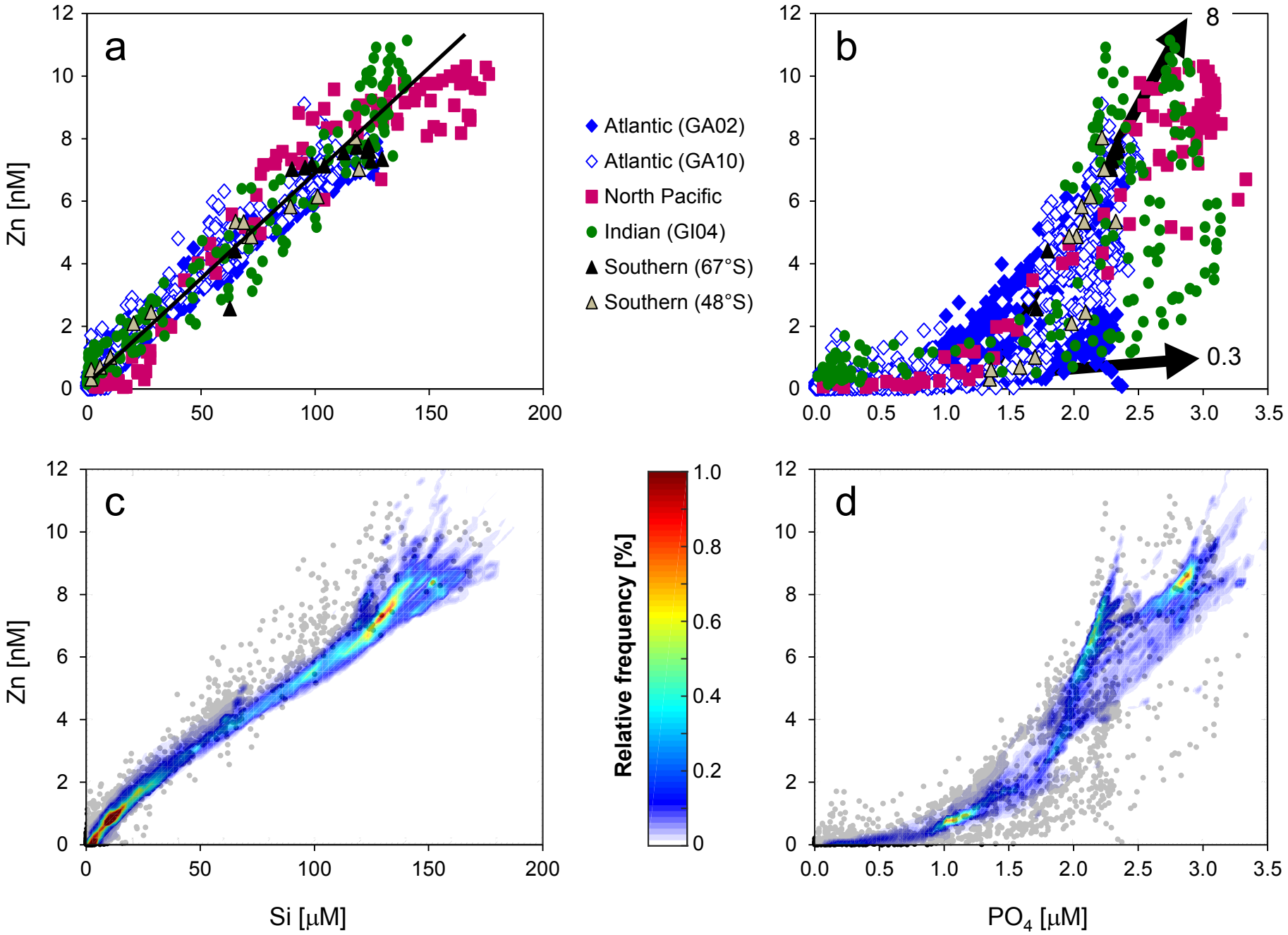
a
b
c
d
Zn [nM]
Si [µM]
PO4 [µM]
Relative frequency [%]
Atlantic (GA02)
Atlantic (GA10)
North Pacific
Indian (GI04)
Southern (67°S)
Southern (48°S)
8
0.3

SUPPLEMENTARY INFORMATION TO

Silicon and zinc biogeochemical cycles coupled through the Southern Ocean

Derek Vance, Susan H. Little, Gregory F. de Souza, Samar P. Khatiwala, Maeve C. Lohan, Rob Middag

1. Description of the physical and biogeochemical model framework

Ocean general circulation model simulations were carried out using the transport matrix method (TMM) of Khatiwala et al. (2005), which allows the efficient offline simulation of passive tracers in the ocean by making use of transport matrices (TMs) derived from a full three-dimensional ocean general circulation model. Here, we use TMs derived from a coarse-resolution version of the MITgcm (Marshall et al., 1997) with 2.8° × 2.8° lateral resolution and 15 vertical levels, forced with monthly mean climatological fluxes of momentum, heat and freshwater and with weak restoring of surface temperature and salinity to the Levitus climatology (Levitus et al., 1998). Simulations were carried out with annual-mean circulation fields derived from the equilibrium state of the model after 5000 yr integration; thus, seasonal variability is not represented in our simulations. This physical model is coupled to a biogeochemical model that simulates the internal oceanic cycling of phosphorus (as phosphate, PO_4, and dissolved organic phosphorus, DOP), zinc (Zn) and silica (Si). Biogeochemical model simulations were initialized with constant nutrient tracer fields and integrated forward for 5000 model years; the output for model year 5000 is presented herein.

PO_4 cycling: The nutrient-cycling model that forms the basis of our simulations is based on the formulation developed for the OCMIP-2 project (Najjar et al., 2007) and uses PO_4 as its nutrient currency. Phosphate uptake in the surface ocean (≤ 120m water depth) is driven by restoring surface PO_4 concentrations (Najjar et al., 1992; Anderson and Sarmiento, 1995) towards the objectively-analysed annual-mean PO_4 field of World Ocean Atlas 2013 (Garcia et al., 2013) with a restoring timescale of 36.5 days. A fraction (0.67) of PO_4 taken up is immediately shunted towards the production of DOP, whilst the remaining fraction is exported as an implicit particulate flux to depth, which remineralises following a power-law dependency on depth with an exponent of −0.858 (Martin et al., 1987; Berelson, 2001). Any particulate flux reaching the bottom of the water column remineralises within the bottom ocean cell, since we only represent internal oceanic cycling with no sources (or sinks) into (or out of) the ocean. Dissolved organic phosphorus is carried passively with the circulation and decays back to PO_4 with a first-order rate constant of $(0.5\ \text{year})^{-1}$. Mean ocean phosphorus concentration is set to 2.17 μM (calculated from World Ocean Atlas 2013; Garcia et al., 2013), all of which is in the form of PO_4 at t=0; at equilibrium, mean ocean PO_4 concentration is 2.164 μM, whilst mean DOP concentration is 0.006 μM.

Zn cycling: In order to test our mechanistic hypotheses regarding Zn cycling in the ocean, the Zn-cycling model is explicitly coupled to the PO_4-cycling model above. Zn uptake in the surface ocean is related to PO_4 uptake by a dimensionless stoichiometric parameter $r_{Zn:P}$. This surface-ocean uptake

drives an implicit export flux of particulate Zn, which remineralises identically to the implicit particulate P flux, i.e. following a power-law dependency on depth with an exponent of −0.858. Any particulate flux reaching the bottom of the water column remineralises within the bottom ocean cell. The organic speciation of dissolved Zn is represented implicitly by assuming a constant ligand concentration of 1.2 nM with a conditional stability constant of 10^{10} M^{-1}, which reduces the calculation of the concentrations of free Zn (i.e. organically- and inorganically uncomplexed Zn^{2+}) to the solution of a quadratic equation (see below). Varying biogeochemical behaviours of the Zn-cycling model are achieved by the formulation of the stoichiometric parameter $r_{Zn:P}$, as detailed below. Mean ocean Zn concentration is set to 5.4 nM (Chester and Jickells, 2012).

Si cycling: The silicon cycling model is conceptually very similar to the PO_4-cycling model and the Si-cycling model of de Souza et al. (2014, 2015). Dissolved Si uptake in the surface ocean (≤ 120m water depth) is driven by restoring surface Si concentrations towards the objectively-analysed annual-mean Si field of World Ocean Atlas 2013 with a restoring timescale of 36.5 days. This surface-ocean uptake drives an implicit particulate export flux, which dissolves following an exponential dependency on depth with a length-scale of 1000 m (de Souza et al., 2014; de Souza et al., 2015). Any particulate flux reaching the bottom of the water column remineralises within the bottom ocean cell. Mean ocean Si concentration is set to 92 μM (calculated from World Ocean Atlas 2013; Garcia et al., 2013). It is important to note that in our model formulation, Si cycling is *entirely biogeochemically independent* of PO_4 and Zn cycling.

2. Parameterisation of Zn uptake

2.1. Rationale

The hypothesis proposed in this study is based on the observation that Southern Ocean diatoms possess a Zn quota (relative to P) that is 5 to 13 times higher than that of average oceanic phytoplankton. Export of organic matter with such an elevated Zn:P ratio in the Southern Ocean could thus lead to a decoupling of the large-scale distributions of Zn and PO_4 in a similar manner to that proposed by Sarmiento et al. (2004) for Si, without requiring any mechanistic coupling between Zn and Si.

A potential explanation of the high Zn quota of Southern Ocean phytoplankton may lie in Sunda and Huntsman's (1992) observation of the dependence of phytoplankton Zn uptake (and Zn quota) on the ambient concentration of free Zn (i.e. Zn^{2+}). From the limited observations of Zn speciation, the surface waters of the Southern Ocean represent the only euphotic zone where total dissolved Zn concentrations exceed those of the chelating organic ligand, allowing Zn^{2+} concentrations to rise (Baars and Croot, 2011). In our simulations, we assess the influence of such a Zn^{2+}-dependence of Zn uptake on the large-scale distribution of Zn. We do this via two idealized models of Zn uptake, in which this uptake is either (a) a linear function of total dissolved Zn concentration (model version

LIN) or (b) a non-linear function of Zn^{2+} concentration as in Sunda and Huntsman (1992; model version NONLIN).

2.2. Model description

In both Zn model versions used herein, the implicit assumption is that oceanic concentration of the chelating ligand (denoted L) is constant at 1.2 nM. The existing sparse observations of Zn-complexing ligand concentrations in the ocean (Donat and Bruland, 1990; Bruland, 1989; Ellwood and van den Berg, 2000; Ellwood, 2004; Lohan et al., 2005; Baars and Croot, 2011) do bear witness to some variability, although only to a limited extent (approximately 0.6–2.4 nM) and without any systematic variation.

Model version LIN was motivated by (i) the wish to maximise model simplicity in order to ease interpretation and (ii) the observation that the non-saturating Michaelis-Menten dependence of Zn uptake on Zn^{2+} (see model NONLIN below), together with the simple quadratic dependence of Zn^{2+} on total dissolved Zn (given constant L) combine to produce a near-linear dependence of Zn uptake on total dissolved Zn (see Fig. S1), making this formulation a good first approximation. In this model version, the stoichiometric parameter $r_{Zn:P}$ (mol/mol) that couples the uptake of Zn to that of PO_4 is given by:

$$r_{Zn:P} = m_{Zn} \cdot Zn^T \quad \text{(Eqn. 1)}$$

where Zn^T is total dissolved Zn and m_{Zn} is a prescribed slope. The Zn uptake term is then simply calculated as:

$$J_{Zn}^{uptake} = r_{Zn:P} \cdot J_{PO4}^{uptake} \quad \text{(Eqn. 2)}$$

Model version NONLIN was motivated by (i) the wish to maximise fidelity to observations of Zn uptake in culture experiments (Sunda and Huntsman, 1992), and (ii) the inability of LIN to reproduce the location and position of the latitudinal gradient in surface Zn concentrations (see Section 3.2). Following the formulation of Sunda and Hunstman, in this model version the stoichiometric parameter that couples Zn uptake to PO_4 uptake is a non-saturating Michaelis-Menten-type function of Zn^{2+}, i.e. the sum of a Michaelis-Menten function and a linear dependency (the so-called "two-site" model):

$$r_{Zn:P} = \frac{a_{Zn} \cdot Zn^{2+}}{b_{Zn} + Zn^{2+}} + c_{Zn} \cdot Zn^{2+} \quad \text{(Eqn. 3)}$$

where parameters a_{Zn}, b_{Zn} and c_{Zn} are constants analogous to maximum uptake rate, half-saturation constant and non-saturable uptake rate, respectively. The concentration of Zn^{2+} is calculated from the implicit concentration of non-ligand-bound Zn (Zn') following the simple relationship:

$$Zn^{2+} = Zn'/\alpha \quad \text{(Eqn. 4)}$$

where α = 2.1 is the inorganic side-reaction coefficient for Zn in seawater (Ellwood and Van den Berg, 2000). In its turn, Zn' is calculated as the positive root of the quadratic equation that follows from the mass balance of Zn and the chelating ligand L:

$$K_L \cdot (Zn')^2 + (K_L L^T - K_L Zn^T + 1) \cdot Zn' - Zn^T = 0 \quad \text{(Eqn. 5)}$$

where K_L = 10^{10} M^{-1} is the conditional stability constant for the chelation of Zn by the ligand L, and L^T = 1.2 nM is the concentration of total ligand L (i.e., both unbound and Zn-bound L). Finally, as in model LIN above, the Zn uptake term is related to PO_4 uptake following Eqn. 2.

2.3. Uptake parameter choices

In model version NONLIN, a range of values for the parameters a_{Zn}, b_{Zn} and c_{Zn} in Eqn. 3 was obtained by fitting this function to culture data from five diatom and coccolithophorid species/clones from Sunda and Huntsman (1992). Of these parameter sets, the values for the diatom *Thalassiosira oceanica* produce an uptake dependence that lies squarely in the centre of the species variability (Fig. S2). In model version LIN, the standard value of m_{Zn} in Eqn. 1 was set so as to roughly reproduce the dependence of rZn:P on ZnT in Eqn. 3 when using the parameters for *T. oceanica*. Parameters and key statistical metrics for the 11 sensitivity simulations carried out are listed in Table S1.

3. Results

3.1. Global metrics

In the following, we illustrate the degree of similarity between tracer fields using Taylor diagrams (Taylor, 2001), which provide a concise statistical summary of the similarity between two three-dimensional fields as a single point (defined by the normalised centred root mean square (RMS) difference, correlation coefficient, and relative standard deviation of these two fields) on a polar-style graph. We use these diagrams both to quantify model skill at reproducing the global distributions of PO_4 and Si as represented by World Ocean Atlas 2013 (WOA13), as well as to compare the similarity of the global oceanic Zn fields simulated by our two model variants (and corresponding parameter-sensitivity simulations). For all diagrams shown herein, tracer fields are first interpolated to the model grid if required (e.g. for the WOA13 fields), and statistics calculated after weighting the tracer concentration by the corresponding model cell volume (Taylor, 2001).

Figure S3 compares the results of our PO_4 and Si cycling models to the corresponding three-dimensional tracer fields from WOA13. Both models reproduce the large-scale oceanic macronutrient patterns with good fidelity: the correlation coefficient R between model output and WOA13 is 0.87 for PO_4 and 0.92 for Si, whilst the corresponding normalised centred RMS difference $\hat{E}'$ is 0.57 for PO_4 and 0.41 for Si. The PO_4 field simulated by our OCMIP-2-type PO_4–DOP cycling model compares favourably with other ocean biogeochemistry general circulation models of this type (see e.g. Gnanadesikan et al., 2004).

Figure S4 presents a sensitivity analysis for our Zn cycling model variants, in order to illustrate underlying systematics that produce a Zn distribution that mimics either that of PO_4 or of Si. In order to do this most clearly, Fig. S4 compares the model Zn tracer field with *simulated* PO_4 and Si tracer fields scaled by the ratio between the mean ocean concentrations of these species (i.e. Zn is compared

with $(\overline{Zn}/\overline{PO_4}) \cdot PO_4$ and $(\overline{Zn}/\overline{Si}) \cdot Si$, where the overbar denotes an average over the entire ocean), in order to explore the mechanistic systematics internal to the model (see also Table S1). Model formulations and parameter choices that produce a more Si-like distribution of Zn will thus exhibit a lower RMS error and plot closer towards the "bullseye" of the Taylor diagram. Figure S4 shows that, for both formulations of the dependency of Zn uptake on Zn concentration (i.e. model versions LIN and NONLIN), differing choices of parameter values can lead to very different large-scale Zn distributions. Furthermore, it shows that certain choices of model formulation and parameter values produce Zn distributions that are *very* similar to the Si field (red symbols close to normalised standard deviation of 1 and with correlation coefficients >0.95; e.g. Simulation 11), whilst other choices may instead produce PO_4-like distributions (green symbol for Simulation 1 in the same region).

3.2. Surface-ocean metrics

The Taylor diagrams discussed above are an excellent way of quantifying global similarity in tracer fields. However, due to the fact that cells are weighted by their volume in constructing the relevant statistics, these diagrams are not very sensitive to changes in the surface and upper ocean, whose volume and nutrient concentrations are small relative to those of the deep ocean. Thus, in the following, we focus on a few surface ocean metrics to illustrate the sensitivity of our Zn-cycling model to uptake formulation and parameter choices.

Figure S5 shows the zonal average surface Zn concentration produced by the various sensitivity simulations for which global metrics are presented in Fig. S4 above. Note that whilst model PO_4 and Si distributions are prescribed by the surface-restoring production scheme used by the respective models, the simulated surface Zn field is free to evolve based on the interplay between Zn uptake (which is dependent on PO_4 uptake via Eqn. 2), regeneration and the physical circulation. The fields simulated by model variants LIN (Fig. S5a) and NONLIN (Fig. S5b) are compared to an "ideal" Si-like Zn field that scales as $(\overline{Zn}/\overline{Si}) \cdot Si$ (i.e. one that is linearly correlated with model Si). In Fig. S5a, it can be seen that variant LIN struggles to simultaneously reproduce the low concentrations at mid- to low-latitudes, high concentrations in the subpolar and polar oceans, and sharp latitudinal surface gradient centered at around 55°S of the "ideal Zn" field. The sensitivity simulation that produces the most Si-like Zn distribution at the global scale (Simulation 6) strongly underestimates surface Zn concentrations south of about 60°S (by about 30%), but does place the zonally-averaged Southern Ocean surface Zn gradient at approximately the right position. In comparison, the model variant NONLIN (Fig. S5b) is capable of not only producing the sharp Zn concentrations differences between the low- and high-latitude surface oceans, but of maintaining this gradient even when the zonally-averaged Southern Ocean surface Zn gradient is moved southwards towards (but not quite reaching) 55°S. The best-performing sensitivity simulation of this model variant (Simulation 11) produces surface Southern Ocean Zn concentrations within a few percent of the zonally averaged "ideal Zn" and places the strong latitudinal Zn gradient only a few degrees too far north. Relative to this "ideal Zn", the model does appear to underestimate low-latitude surface Zn concentrations, although observations

show that Zn concentrations in the low-latitude ocean can be extremely low (e.g. <0.1 nM in the low-latitude Atlantic Ocean; Wyatt et al., 2014).

By combining the simulated Zn fields shown in Fig. S5 with Eqns. 3-5, we can diagnose the Zn:P of uptake simulated by these model variants (Fig. S6). From a comparison of Fig. S6 with Figs. S4 and S5, it is clear that the sensitivity simulations in which there is great latitudinal plasticity in $Zn:PO_4$ uptake ratio, especially with a sharp gradient between the mid- to low-latitude and the subpolar/polar oceans poleward of 40°S, are the most successful at producing a surface and global-ocean Zn distribution that is similar to that of Si. The variability of $Zn:PO_4$ uptake simulated in our sensitivity simulations is well within the observed plasticity of Zn:P as compiled, for instance, by Twining and Baines (2013).

4. Conclusions

Our sensitivity simulations illustrate the wide variety of elemental distributions that can be simulated as the result of varying a few model parameters that control the stoichiometry of elemental uptake in the surface ocean. The Zn distributions simulated by our suite of models thus ranges from being similar to PO4 to being tightly and near-linearly correlated with Si (Fig. S4). The particular importance of Southern Ocean uptake stoichiometry in controlling this variation is shown systematically in Fig. S7, which plots the export-weighted mean $Zn:PO_4$ uptake ratio in the Southern Ocean (>50°S) against the normalised centred RMS difference between the Zn fields simulated by our 11 sensitivity simulations and the simulated Si and PO_4 fields (scaled by the appropriate ocean-mean elemental ratio, as detailed in Section 3.1). It can be seen that elevated $Zn:PO_4$ uptake in the Southern Ocean systematically results in a more "Si-like" global Zn distribution, regardless of the specifics of our model formulation (LIN vs. NONLIN). As discussed in Section 3.2, the simulation that best reproduces both global (Fig. S4) and surface (Fig. S5) Zn distributions is Simulation 11 (Table S1), a version of model variant NONLIN in which the $Zn:PO_4$ of uptake increases rapidly at low Zn^{2+} and almost saturates thereafter; this feature seems to produce a sharp gradient in $Zn:PO_4$ of uptake across the subpolar oceans (Fig. S6) and may be responsible for the model's skill at reproducing the sharp surface gradient in Zn *concentrations* here (Fig. S5). It is this simulation for which we show results in the main text (Fig. 3).

At this juncture it is worth explicitly noting once again that the similarity in Zn and Si fields in our simulations comes about *without* any coupling between Zn and Si in the models and *despite* the difference in their regeneration lengthscales, since Zn is cycled identically to PO_4 in our models. Rather, this similarity is driven by the geographically collocated, but mechanistically unrelated, strong uptake of Zn and Si by Southern Ocean phytoplankton communities.

Table S1. Details of the sensitivity simulations performed, including key parameter values and normalised centred RMS difference ($\hat{E}$') of the appropriately scaled model Zn field to simulated Si and PO_4 fields (see Section 3.1).

Simu-lation	Model variant	Description	Key parameter values			$\hat{E}$'	
			m_{Zn} [mol:mol/μM]			vs. Si	vs. PO_4
1	LIN	0.25× standard slope	0.339			0.53	0.16
2	LIN	0.5 standard slope	0.679			0.43	0.37
3	LIN	Standard slope (Eqn. 1 fit to *T. oceanica*)	1.357			0.34	0.59
4	LIN	1.5× standard slope	2.036			0.30	0.70
5	LIN	2× standard slope	2.714			0.27	0.77
6	LIN	3× standard slope	4.071			0.26	0.86
			a_{Zn} [mol:mol]	b_{Zn} [μM]	c_{Zn} [mol:mol/μM]		
7	NONLIN	Eqn. 3 fit to *E. huxleyi A1383*	2.4×10^{-3}	4.0×10^{-5}	4.7	0.30	0.71
8	NONLIN	Eqn. 3 fit to *T. weissflogii*	1.6×10^{-3}	1.7×10^{-5}	4.0	0.32	0.66
9	NONLIN	Eqn. 3 fit to *T. oceanica*	1.25×10^{-3}	1.0×10^{-5}	2.9	0.35	0.6
10	NONLIN	Eqn. 3 fit to *T. pseudonana*	1.2×10^{-3}	8.0×10^{-6}	1.7	0.39	0.52
11	NONLIN	Eqn. 3 fit to *E. huxleyi BT6*	6.0×10^{-3}	3.0×10^{-5}	0.32	0.26	0.81

Fig. S1

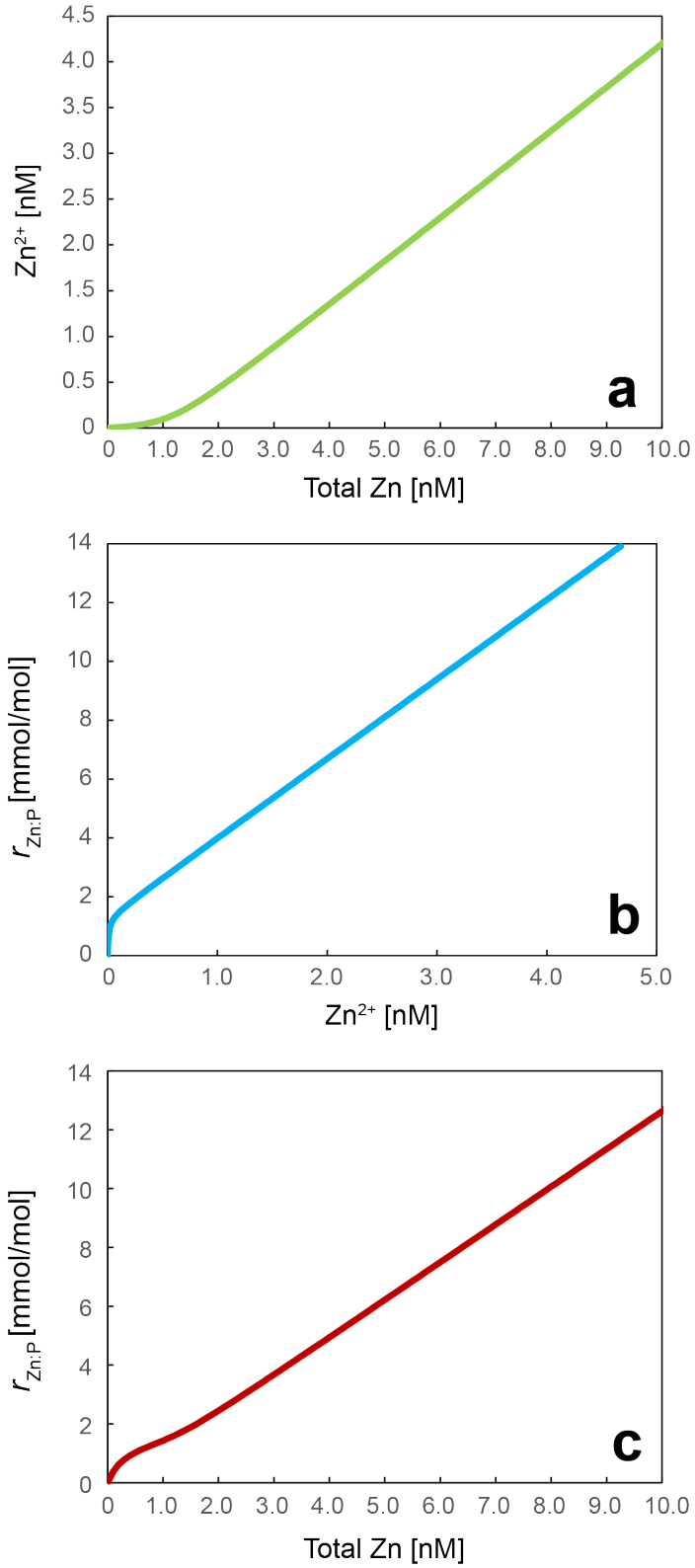

Fig. S1: Systematics of Zn speciation and Zn:P uptake. Relationship between (a) concentration of Zn^{2+} and total Zn in the presence of a chelating organic ligand (ligand concentration 1.2 nM, conditional stability constant 10^{10} M^{-1}) and (b) the non-linear "two-site" dependence of P-specific Zn uptake $r_{Zn:P}$ on Zn^{2+} concentration, based on culture data of Sunda and Huntsman (1992). These two dependencies combine to produce the near-linear dependence of $r_{Zn:P}$ on total Zn in panel *c*.

Fig. S2

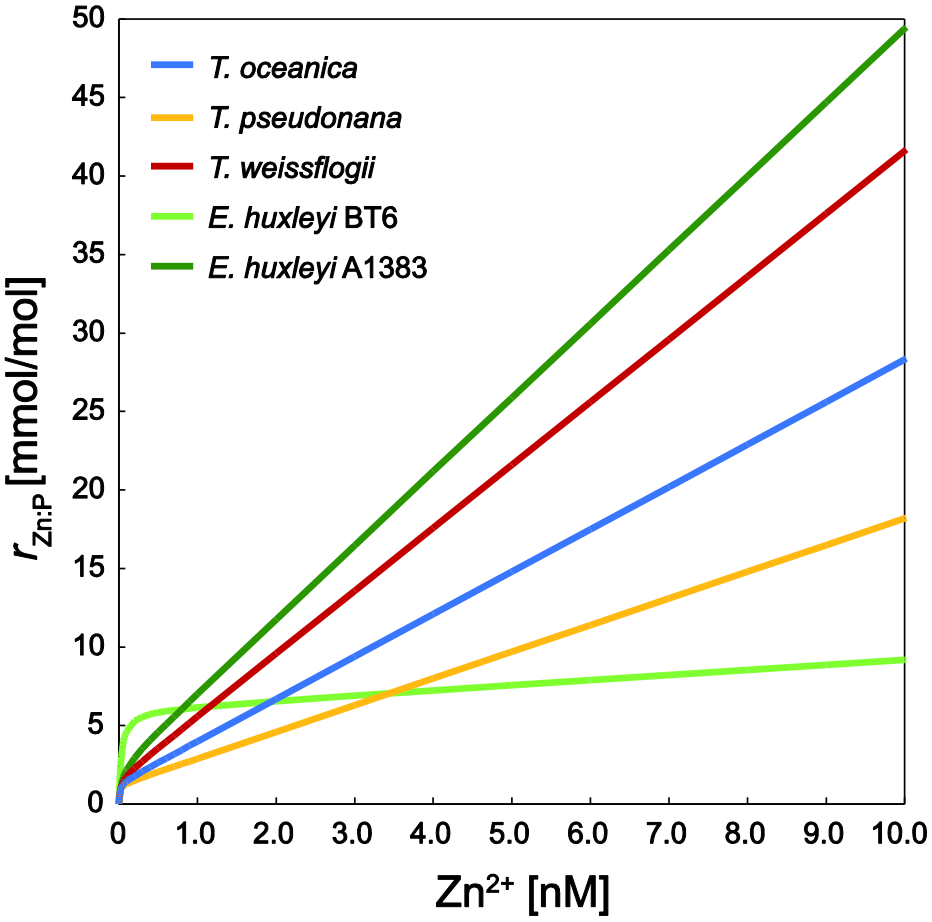

Fig. S2: Variability in specific Zn uptake dependency in phytoplankton. "Two-site" model curves (Eqn. 3) fit to culture data from Sunda and Huntsman (1992). Considerable variability is observed, both between genera and between clones of the same species. We apply this large observed variability in the dependence of $r_{Zn:P}$ on Zn^{2+} concentrations in 5 parameter sensitivity simulations of the model variant NONLIN in order to assess the extent to which surface uptake processes may affect the large-scale Zn distribution.

Fig. S3

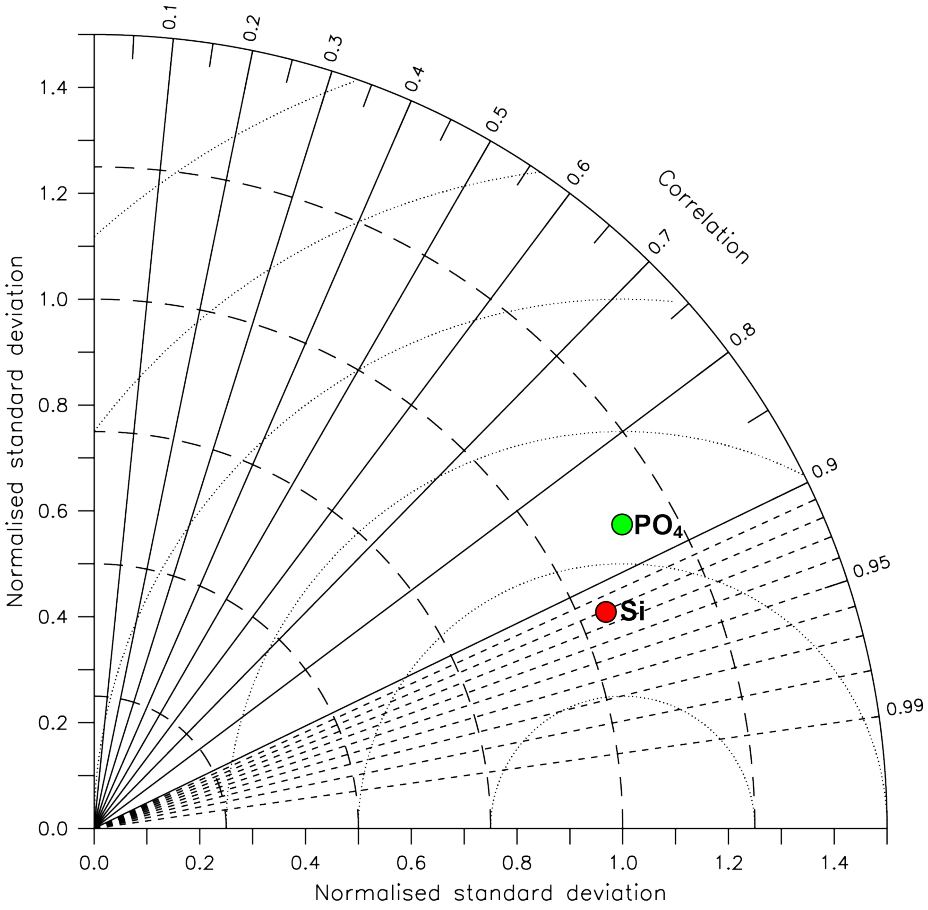

Fig. S3: Evaluation of PO_4 and Si model skill. Volume-weighted Taylor diagram comparing the three-dimensional simulated PO_4 and Si tracer fields to the corresponding objectively-analysed fields in World Ocean Atlas 2013 (Garcia et al., 2013). Both model fields exhibit good fidelity to the data product, with normalised standard deviations close to 1 and correlation coefficients above 0.85.

Fig. S4

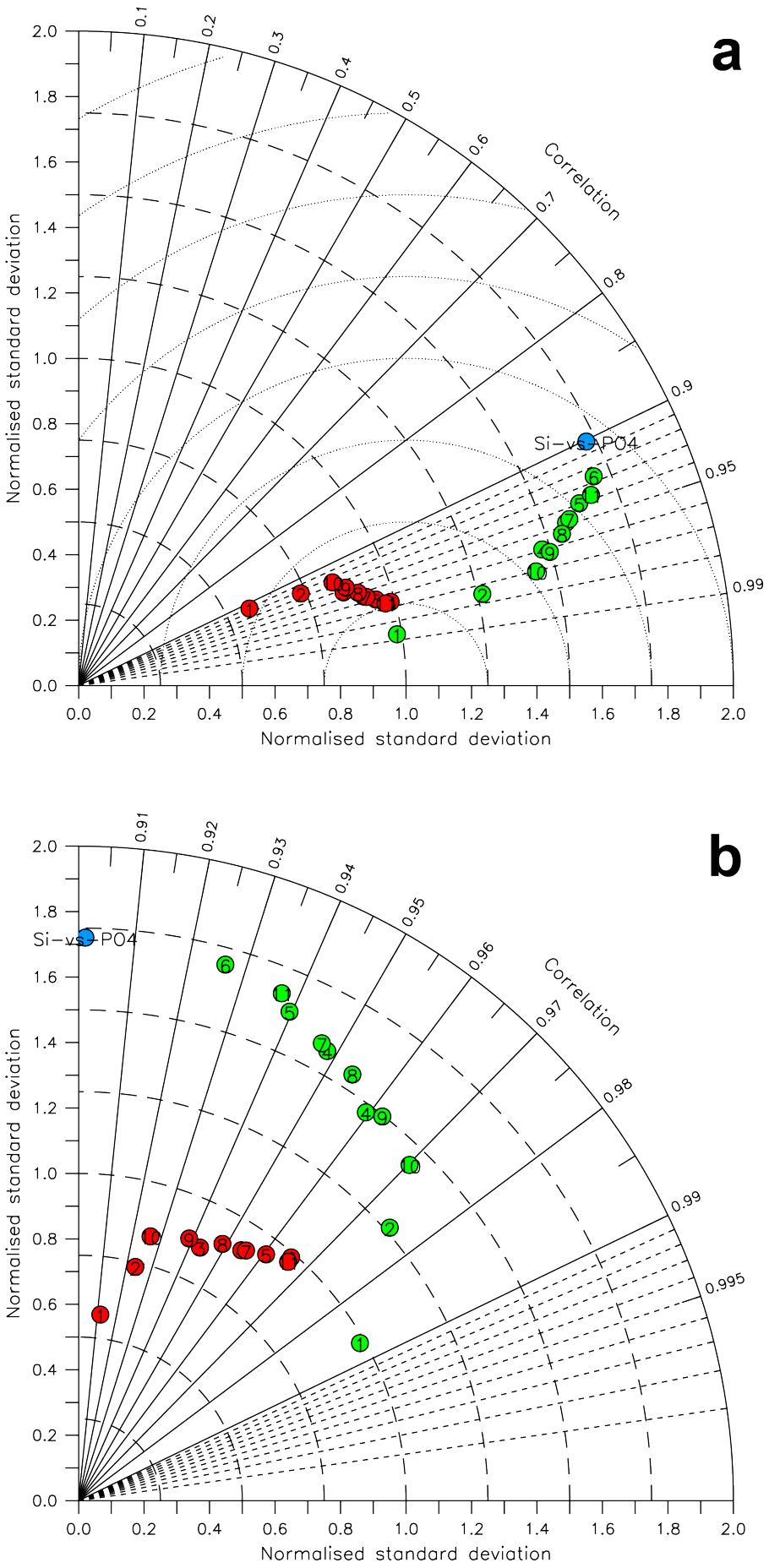
a
b
Correlation
Normalised standard deviation
Si–vs–PO4
0.1
0.2
0.3
0.4
0.5
0.6
0.7
0.8
0.9
0.95
0.99
0.91
0.92
0.93
0.94
0.96
0.97
0.98
0.995
0.0
0.2
0.4
0.6
0.8
1.0
1.2
1.4
1.6
1.8
2.0

Fig. S4: Comparison of simulated Zn distributions to model Si and PO_4 fields. Each circle in the volume-weighted Taylor diagram above represents a parameter-sensitivity simulation of the Zn cycling model variants LIN (6 simulations) and NONLIN (5 simulations) and compares the appropriately scaled three-dimensional Zn field to the simulated Si field (red circles) or PO_4 field (green circles; see Section 3.1). The blue circle is included as reference and illustrates the degree of similarity between the appropriately scaled simulated Si and PO_4 fields. It can be seen that, depending on parameter choices in either of the two model variants, the simulated Zn distribution may be either similar to the Si tracer field (red circles close to a normalised standard deviation of 1 and with high correlation coefficient) or to the PO_4 tracer field (green circle in the same region). Panel *b* presents the same results as panel *a* with an enlarged scale for the correlation coefficient (0.9 – 1.0) for better clarity. See Table S1 for details of the simulations.

Fig. S5

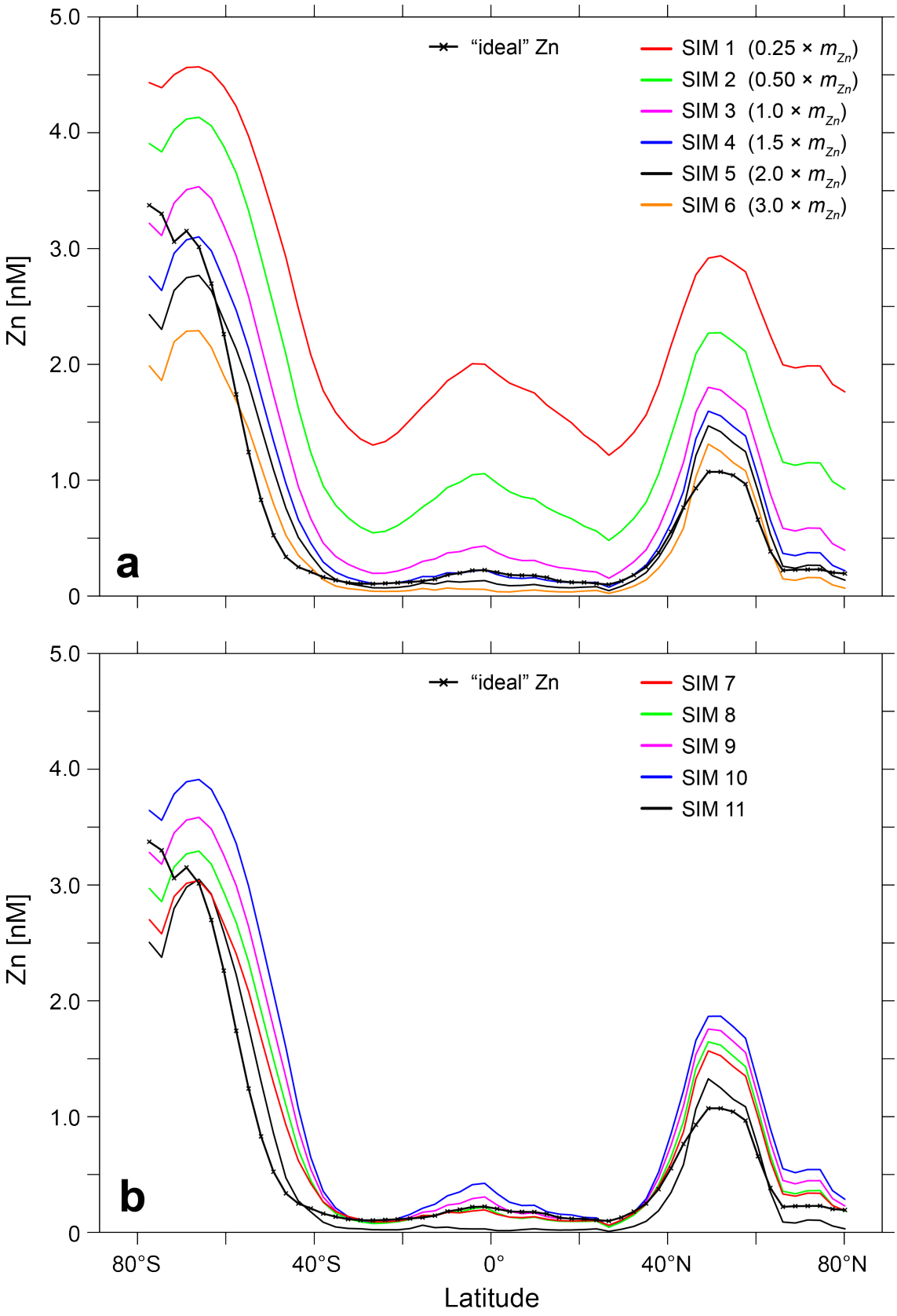

Fig. S5: Zonal mean surface Zn concentration. Results from the parameter sensitivity simulations of the two model variants (a) LIN and (b) NONLIN are shown relative to an hypothetical "ideal" Zn distribution that scales linearly with Si. See Table S1 for details of the simulations.

Fig. S6

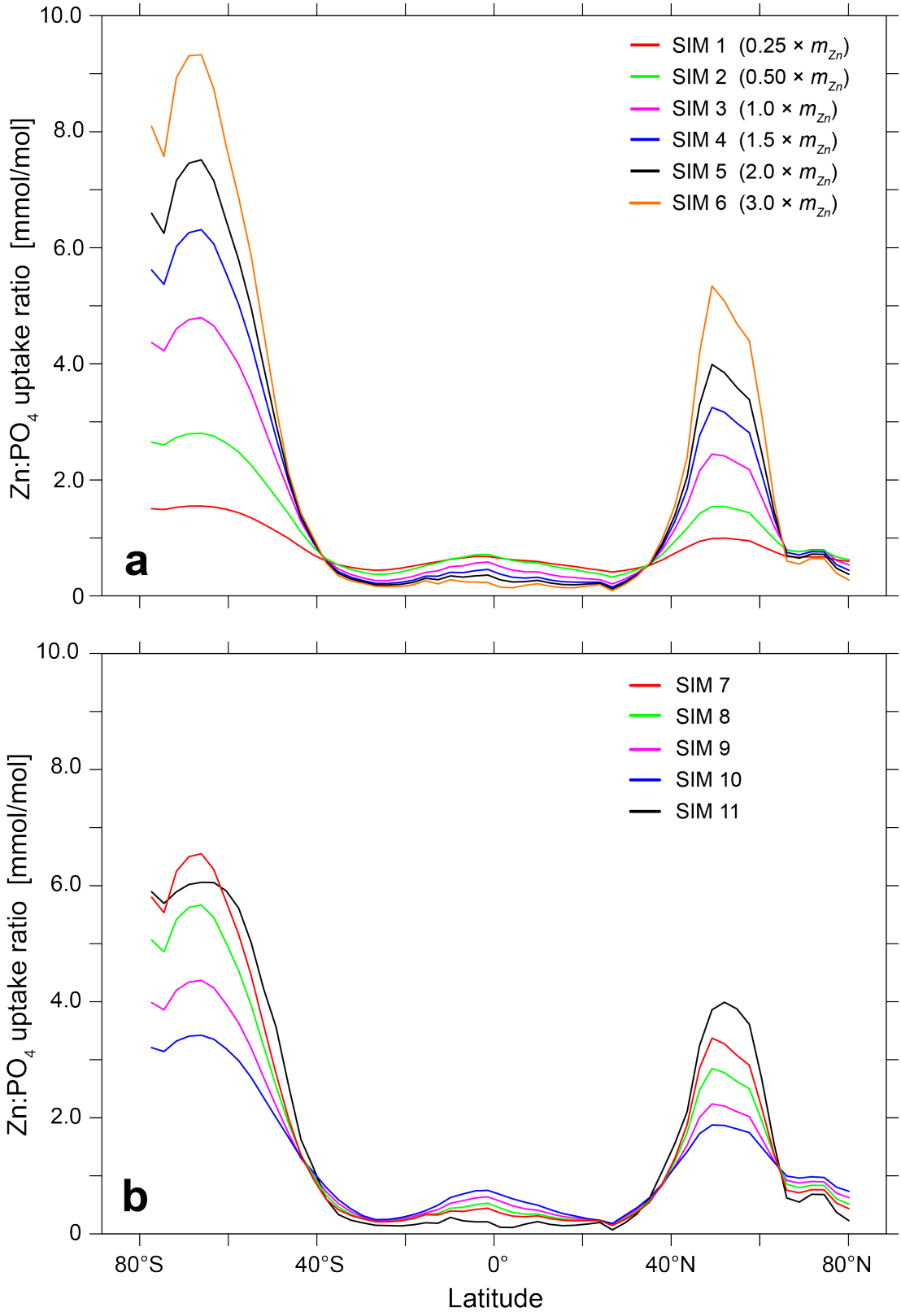

Fig. S&: Zonal mean $Zn:PO_4$ uptake ratio. Both model variants (a) LIN and (b) NONLIN can exhibit strong latitudinal variability in $Zn:PO_4$ uptake depending on the choice of parameter values. Comparison with Figs. S4 and S5 above reveals that simulations with greater latitudinal gradients in $Zn:PO_4$ of uptake produce surface *and* global ocean Zn distributions that more closely resemble the Si distribution (see also Fig. 3 of the main text). See Table S1 for details of the simulations.

Fig. S7

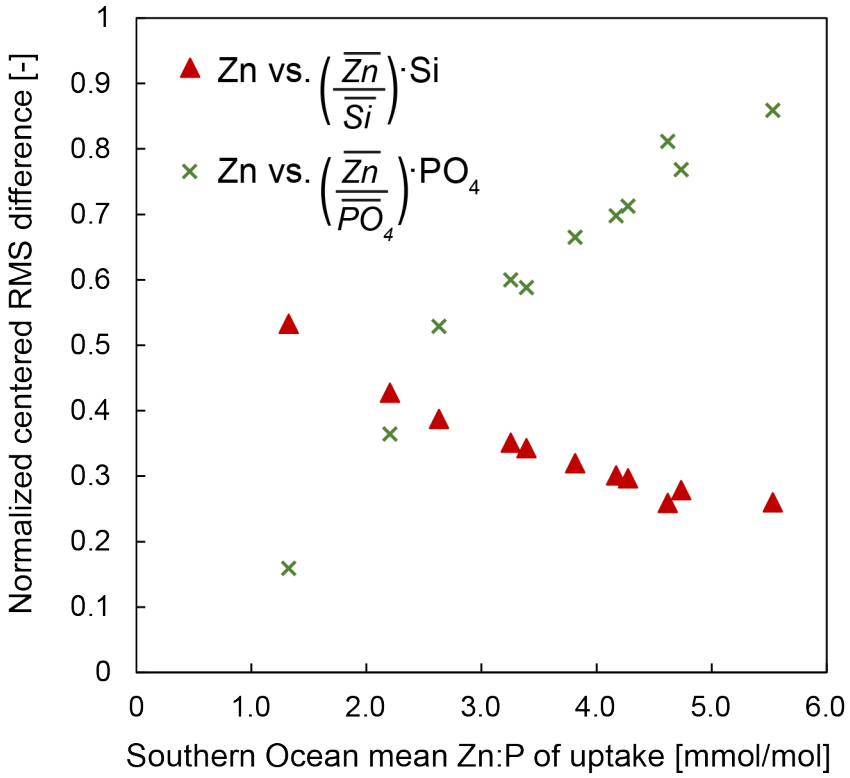

Fig. S7: Systematics of the control of Southern Ocean uptake stoichiometry on global Zn distribution. As the export-weighted mean Zn:P uptake ratio in the Southern Ocean (>50°S) increases in our simulations, the simulated Zn field becomes increasingly "Si-like", whilst its similarity to the simulated PO_4 field decreases, as reflected by the increase in normalised centred RMS difference $\hat{E}'$ between the two fields. Export-weighted means were calculated as the ratio of the total Zn export flux south of 50°S to that of P.

References

Anderson, L.A., Sarmiento, J.L., 1995. Global ocean phosphate and oxygen simulations. *Glob. Biogeochem. Cyc.* 9, 621-636.

Baars, O., Croot, P.L., 2011. The speciation of dissolved zinc in the Atlantic sector of the Southern Ocean. *Deep Sea Res. II* 58, 2720-2732.

Berelson, W.M., 2001. The flux of particulate organic carbon into the ocean interior: a comparison of four US JGOFS regional studies. *Oceanogr.* 14, 59-67.

Bruland, K.W., 1989, Complexation of zinc by natural organic ligands in the central North Pacific. *Limnol. Oceanogr.* 34, 269-285.

Chester, R., Jickells, T., 2012. Marine Geochemistry, 3rd ed. Wiley-Blackwell, Chichester.

de Souza, G.F., Slater, R.D., Dunne, J.P., Sarmiento, J.L., 2014. Deconvolving the controls on the deep ocean's silicon stable isotope distribution. *Earth Planet. Sci. Lett.* 398, 66-76.

de Souza, G.F., Slater, R.D., Hain, M.P., Brzezinski, M.A., Sarmiento, J.L., 2015. Distal and proximal controls on the silicon stable isotope signature of North Atlantic Deep Water. *Earth Planet. Sci. Lett.* 432, 342-353.

Donat, J.R., Bruland, K.W., 1989. A comparison of two voltametric technqiues for determining zinc speciation in Northeast Pacific Ocean waters. *Mar. Chem.* 28, 301-323.

Ellwood, M.J., 2004. Zinc and cadmium speciation in sub-Antarctic waters east of New Zealand. *Mar. Chem.* 87, 37-58.

Ellwood, M.J., van den Berg, C.M.G., 2000. Zinc speciation in the Northeastern Atlantic Ocean. *Mar. Chem.* 68, 295-306.

Garcia, H.E., Locarnini, R.A., Boyer, T.P., Antonov, J.I., Baranova, O.K., Zweng, M.M., Reagan, J.R., Johnson, D.R., 2013. World Ocean Atlas 2013, Volume 4: Dissolved Inorganic Nutrients (phosphate, nitrate, silicate), Levitus, S. (Ed.), *NOAA Atlas NESDIS 76*, Silver Spring, MD.

Gnanadesikan, A., Dunne, J., Key, R., Matsumoto, K., Sarmiento, J.L., Slater, R., Swathi, P.S., 2004. Oceanic ventilation and biogeochemical cycling: Understanding the physical mechanisms that produce realistic distributions of tracers and productivity. *Glob. Biogeochem. Cyc.* 18, doi:10.1029/2003GB002097.

Khatiwala, S., Visbeck, M., Cane, M.A., 2005. Accelerated simulation of passive tracers in ocean circulation models. *Ocean Modell.* 9, 51-69.

Levitus, S., et al., 1998. World Ocean Database 1998, *NOAA Atlas NESDIS* 18, NOAA, Silver Spring, MD.

Lohan, M.C., Crawford, D.W., Purdie, D.A., Statham, P.J., 2005. Iron and zinc enrichments in the northeastern subarctic Pacific: ligand production and zinc availability in response to phytoplankton growth. *Limnol. Oceanogr.* 50, 1428-1437.

Marshall, J., Adcroft, A., Hill, C., Perelman, L., Heisey, C., 1997. A finite-volume, incompressible Navier-Stokes model for studies of the ocean on parallel computers. *J. Geophys. Res. Oceans* 102, 5733-5752.

Martin, J.H., Knauer, G.A., Karl, D.M., Broenkow, W.W., 1987. VERTEX: carbon cycling in the northeast Pacific. *Deep Sea Res.* 34, 267-285.

Najjar, R.G., Sarmiento, J.L., Toggweiler, J.R., 1992. Downward transport and fate of organic matter in the ocean: Simulations with a general circulation model. *Glob. Biogeochem. Cyc.* 6, 45-76.

Najjar, R.G., et al., 2007. Impact of circulation on export production, dissolved organic matter, and dissolved oxygen in the ocean: Results from Phase II of the Ocean Carbon-cycle Model Intercomparison Project (OCMIP-2). *Glob. Biogeochem. Cyc.* 21, doi: 10.1029/2006gb002857.

Sarmiento, J.L., Gruber, N., Brzezhinski, M.A., Dunne, J.P., 2004. High latitude controls of thermocline nutrients and low latitude biological productivity. *Nature* 427, 56-60.

Sunda, W.G., Huntsman, S.A., 1992. Feedback interactions between zinc and phytoplankton in seawater. *Limnol. Oceanogr.* 37, 25-40.

Taylor, K.E., 2001. Summarizing multiple aspects of model performance in a single diagram. *J. Geophys. Res. Atm.* 106, 7183-7192.

Twining, B.S., Baines, S.B., 2013. The trace metal composition of marine phytoplankton. *Ann. Rev. Mar. Sci.* 5, 191-215.

Wyatt, N.J., Milne, A., Woodward, E.M.S., Rees, A.P., Browning, T.J., Bouman, H.A., Worsfold, P.J., Lohan, M.C., 2014. Biogeochemical cycling of dissolved zinc along the GEOTRACES South Atlantic transect GA10 at 40°S. *Glob. Biogeochem. Cyc.* 28, doi: 10.1002/2013gb004637.